



Short communication

Synthesis, sinterability and ionic conductivity of nanocrystalline Pr-doped $\text{La}_2\text{Mo}_2\text{O}_9$ fast oxide-ion conductors

A. Subramania ^{a,*}, T. Saradha ^a, S. Muzhumathi ^b^a Advanced Materials Research Laboratory, Department of Industrial Chemistry, Alagappa University, Karaikudi 630 003, India^b Fuel Cell Division, Central Electrochemical Research Institute, Karaikudi 630 006, India

Received 28 October 2006; accepted 30 January 2007

Available online 25 February 2007

Abstract

A new series of nanocrystalline $\text{La}_{2-x}\text{Pr}_x\text{Mo}_2\text{O}_9$ ($0.2 \leq x \leq 0.8$) powders are synthesized through the pyrolysis of polyacrylate salt precursors prepared via *in situ* polymerization of the metal salts and acrylic acid. The polymeric precursors are characterized by thermogravimetric and differential thermal analysis (TG/DTA) to determine the thermal decomposition and crystallization temperature, which is found to be at 510 °C. X-ray diffraction analysis indicates that the substitution of La by Pr preserves the single-phase $\text{La}_2\text{Mo}_2\text{O}_9$ structure up to a Pr dopant concentration of $x \leq 0.7$. The particle size and the $\alpha \rightarrow \beta$ phase transition of the Pr-doped $\text{La}_2\text{Mo}_2\text{O}_9$ samples are studied by using a transmission electron microscope (TEM) and differential scanning calorimetry (DSC), respectively. The sintering behaviour of the Pr-doped samples are examined via isothermal and non-isothermal experiments. It demonstrates that the synthesized nanocrystalline powders have good sinterability and a relatively low sintering temperature of 800 °C for 4 h is sufficient to reach ~99% of the theoretical density with good microstructures. Furthermore, the oxide-ion conductivity increases with increasing Pr content and the maximum conductivity is attained at $x=0.5$ in $\text{La}_{2-x}\text{Pr}_x\text{Mo}_2\text{O}_9$.

© 2007 Published by Elsevier B.V.

Keywords: Pr-doped $\text{La}_2\text{Mo}_2\text{O}_9$; Fast oxide-ion conductors; Polymeric precursor; Sintering; Ionic conductivity**1. Introduction**

The development of novel oxide-ion conducting solid electrolytes is of great importance for numerous high-temperature electrochemical applications, such as solid oxide fuel cells (SOFCs), oxygen pumps, electrocatalytic reactors for natural gas conversion, and sensors [1–4]. Solid oxide fuel cells have attracted considerable interest in recent years because of their high efficiency and environmentally friendly operation. Such systems required oxygen-conducting electrolytes and, to date, yttria-stabilized zirconia (YSZ) has been the common choice. This compound exhibits high oxide-ion conductivity at elevated temperatures (850–1000 °C), but high working temperatures cause problems in terms of materials selection and lifetime. Therefore, it is desirable to develop a solid electrolyte that functions well at intermediate temperatures below 800 °C [5,6].

Many other types of fast oxide-ion conductor have been investigated as alternatives to YSZ, e.g., porovskite-type ABO_3 (doped LaGaO_3) [7–9], fluorite-type (stabilized zirconia [10], ceria [11,12]), aurivillius-type (BIMEVOX) [13,14], and pyrochlores [15,16]. $\text{La}_2\text{Mo}_2\text{O}_9$ (commonly known as LAMOX) has also been examined as a new kind of oxide-ion conductor [17,18]. It shows a reversible phase transition from a monoclinic α -polymorph to a cubic β -polymorph at 580 °C [18]. The high-temperature β - $\text{La}_2\text{Mo}_2\text{O}_9$ is a better conductor than the low-temperature α - $\text{La}_2\text{Mo}_2\text{O}_9$, and the ionic conductivity of the β -form is comparable with that of YSZ. Such high ionic conductivity has been explained in terms of the lone-pair concept proposed by Lacorre [19,20].

The phase transition $\beta \rightarrow \alpha$ is one of the main limitations of lanthanum molybdate as an electrolyte in an operative device, because it would cause a drastic drop in the ionic conductivity below 580 °C and electrolyte breakdown due to repeated cycling between the high- and low-temperature polymorphs. Therefore, suppressing this structural transition may be a good way to improve the conducting properties of this material. Several partial substitutions of $\text{La}_2\text{Mo}_2\text{O}_9$ have been carried out

^{*} Corresponding author. Tel.: +91 4565 228836; fax: +91 4565 225202.

E-mail address: a_subramania@yahoo.co.in (A. Subramania).

by replacing both La and Mo by equivalent cations [20–30]. It seems that some of these substitutions may stabilize the β -cubic structure down to room temperature. The additives have failed, however, to increase the ionic conductivity of $\text{La}_2\text{Mo}_2\text{O}_9$ to any significant extent.

This study reports a new series of compounds in the LAMOX family that are formulated by the substitution of Pr for La in the $\text{La}_2\text{Mo}_2\text{O}_9$ parent compound. The nanocrystalline $\text{La}_{2-x}\text{Pr}_x\text{Mo}_2\text{O}_9$ compounds are synthesized by the pyrolysis of La–Pr–Mo polyacrylates precursors prepared via *in situ* polymerization of the metal salts and acrylic acid [31]. The pyrolysis behaviour of the polymeric precursors is studied by thermal (TG/DTA) analysis. The structural properties, particle size and the phase transition of the synthesized products are characterized by means of X-ray diffraction (XRD), transmission electron microscopy (TEM) and differential scanning calorimetry (DSC). In addition, sinterability and ionic conductivity are also investigated.

2. Experimental

Nanocrystalline $\text{La}_{2-x}\text{Pr}_x\text{Mo}_2\text{O}_9$ ($0.2 \leq x \leq 0.8$) powders were prepared by an *in situ* polymerization method using polyacrylates of La, Pr and Mo as the precursor compounds. The polymeric precursors were made by polymerization of an aqueous solution of acrylic acid in presence of $\text{La}(\text{NO}_3)_3$, $\text{Pr}(\text{NO}_3)_3$ and $(\text{NH}_4)_6\text{Mo}_7\text{O}_{24}$ with $(\text{NH}_4)\text{S}_2\text{O}_8$ as the initiator. The typical experimental procedure was first to dissolve the stoichiometric amounts of $\text{La}(\text{NO}_3)_3 \cdot 6\text{H}_2\text{O}$, $\text{Pr}(\text{NO}_3)_3 \cdot 6\text{H}_2\text{O}$ and $(\text{NH}_4)_6\text{Mo}_7\text{O}_{24} \cdot 4\text{H}_2\text{O}$ in triple-distilled water and then pour the solution into an acrylic acid solution (acrylic acid:H₂O = 70:30 wt.%) with constant stirring. To this, a small amount of 5% $(\text{NH}_4)\text{S}_2\text{O}_8$ solution was added as the initiator to promote the polymerization. Under heating at $\sim 80^\circ\text{C}$, well-distributed polyacrylates of La–Pr–Mo were formed. Afterwards, the polyacrylates were dried at 120°C for 1–2 h. The dried polymeric precursor was homogenized in a ceramic mortar and then pyrolyzed at 510°C for 5 h in air at a heating rate of 5°C min^{-1} to eliminate the residual organic phase and to obtain a nanocrystalline $\text{La}_{2-x}\text{Pr}_x\text{Mo}_2\text{O}_9$ powder.

The thermal decomposition of the polymeric precursors was characterized by Perkin-Elmer TG/DTA thermal analysis (Model: Pyris Diamond) over a temperature range of 30–700 °C with a heating rate of 5°C min^{-1} in air.

X-ray powder diffraction (XRD) data were collected at room temperature with a diffractometer (Model: Philips X'Pert MPD®) with Cu K α radiation. The data were recorded in the 2θ -range of 10–70° with a 0.02° step.

The particle size and morphology of the synthesized powder was observed by means of a JEOL transmission electron microscope (Model: 1200 EX).

The phase transition was studied by differential scanning calorimetry (Model: Perkin-Elmer diamond) over the temperature range of 475–600 °C with a heating rate of 5°C min^{-1} in air.

The synthesized nanocrystalline $\text{La}_{2-x}\text{Pr}_x\text{Mo}_2\text{O}_9$ powders were pressed into a pellets of 10 mm diameter and 1.5–2 mm

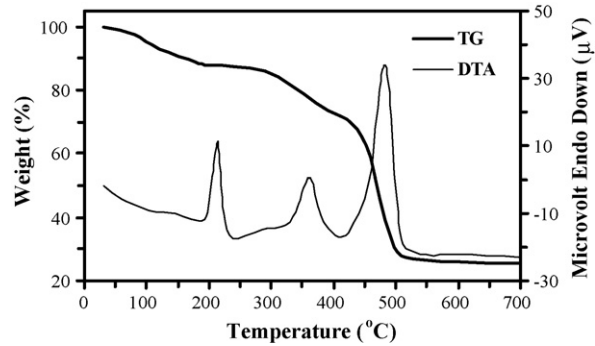


Fig. 1. TG/DTA curves of polyacrylate $\text{La}_{1.5}\text{--Pr}_{0.5}\text{--Mo}_2$ precursor.

thickness, at ~ 150 MPa, using a stainless-steel die. The non-isothermal sintering behaviour of the green pellets were measured with a dilatometer (Model: Netzsch, DIL 402C) from room temperature to 900°C at a heating rate of 5°C min^{-1} and a cooling rate of 5°C min^{-1} . Isothermal sintering was per-

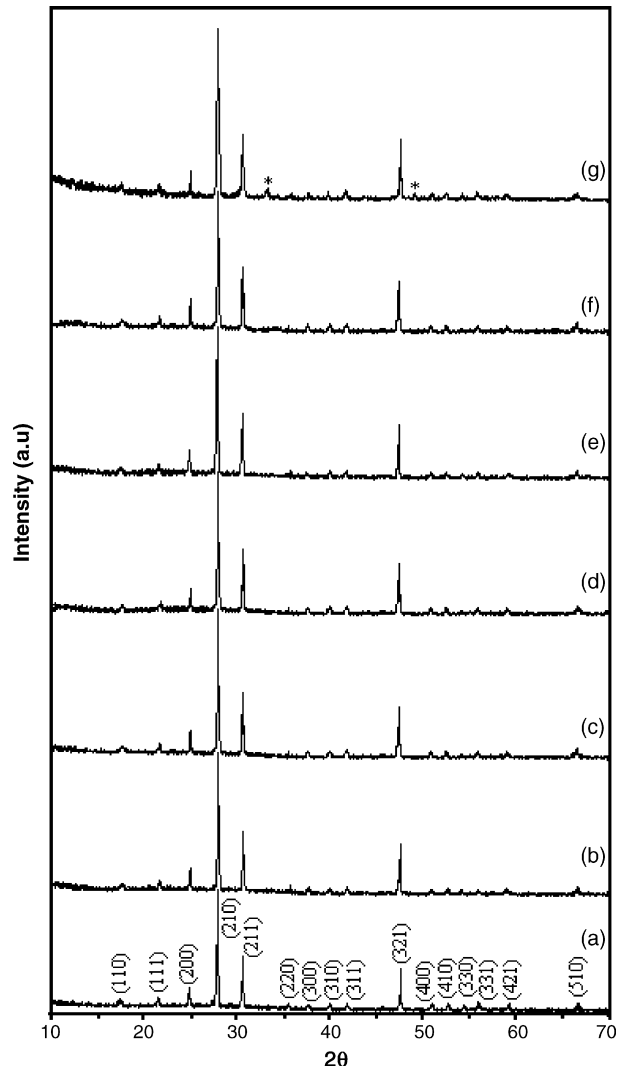


Fig. 2. X-ray diffraction patterns of $\text{La}_{2-x}\text{Pr}_x\text{Mo}_2\text{O}_9$ samples. (a) $\text{La}_{1.8}\text{Pr}_{0.2}\text{Mo}_2\text{O}_9$, (b) $\text{La}_{1.7}\text{Pr}_{0.3}\text{Mo}_2\text{O}_9$, (c) $\text{La}_{1.6}\text{Pr}_{0.4}\text{Mo}_2\text{O}_9$, (d) $\text{La}_{1.5}\text{Pr}_{0.5}\text{Mo}_2\text{O}_9$, (e) $\text{La}_{1.4}\text{Pr}_{0.6}\text{Mo}_2\text{O}_9$, (f) $\text{La}_{1.3}\text{Pr}_{0.7}\text{Mo}_2\text{O}_9$ and (g) $\text{La}_{1.2}\text{Pr}_{0.8}\text{Mo}_2\text{O}_9$.

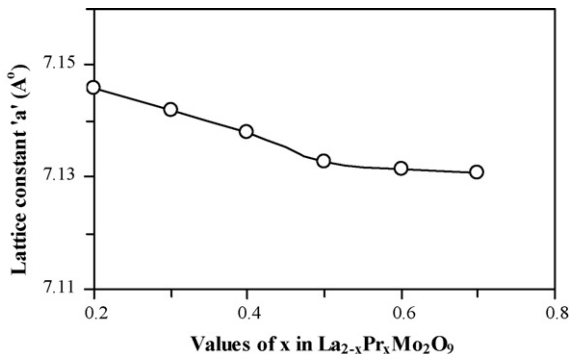


Fig. 3. Variation of lattice parameter of $\text{La}_{2-x}\text{Pr}_x\text{Mo}_2\text{O}_9$ as function of Pr content.

formed on the green pellets using a heating rate of 5°C min^{-1} and a holding time of 4 h at various temperatures (600–900 °C). The density of the sintered pellets was also determined by the Archimedes method using distilled water as the immersion medium. The microstructure of the sintered pellets was monitored with a JEOL scanning electron microscope (Model: JSM-840A).

The ac impedance spectroscopy measurements were carried out in air at temperatures in the range of 300–800 °C on specimens with platinum paste electrodes. A solartron frequency response analyzer (Model: 1260) was used and the frequency range was 0.1 Hz–1 MHz.

3. Results and discussion

To clarify the chemical reaction of the polymeric precursor occurring in the pyrolysis process, TG and DTA analysis of the

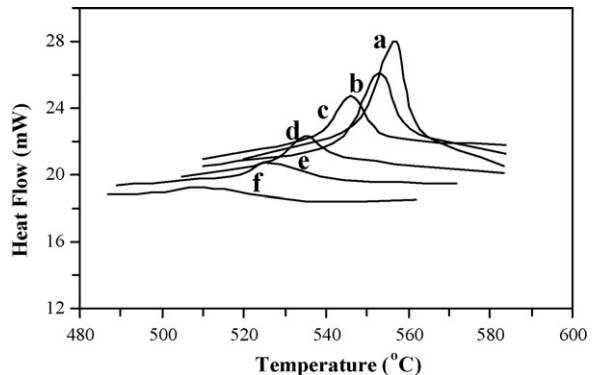


Fig. 5. DSC curves of Pr-doped $\text{La}_2\text{Mo}_2\text{O}_9$ samples. (a) $\text{La}_{1.8}\text{Pr}_{0.2}\text{Mo}_2\text{O}_9$; (b) $\text{La}_{1.7}\text{Pr}_{0.3}\text{Mo}_2\text{O}_9$; (c) $\text{La}_{1.6}\text{Pr}_{0.4}\text{Mo}_2\text{O}_9$; (d) $\text{La}_{1.5}\text{Pr}_{0.5}\text{Mo}_2\text{O}_9$; (e) $\text{La}_{1.4}\text{Pr}_{0.6}\text{Mo}_2\text{O}_9$; (f) $\text{La}_{1.3}\text{Pr}_{0.7}\text{Mo}_2\text{O}_9$.

polyacrylate $\text{La}_{1.5}-\text{Pr}_{0.5}-\text{Mo}_{0.2}$ precursor was conducted. The results are presented in Fig. 1. In the TG curve, three main weight loss domains are observed in the temperature ranges: 30–290, 290–439 and 439–510 °C. The first domain corresponds to the exothermic peak at 214 °C in the DTA curve and is assigned to the decomposition of nitrates. The next two domains are ascribed to the decomposition of La–Pr–Mo polyacrylates into their metal oxides and are accompanied by the exothermic peaks at 363 and 482 °C in the DTA curve. Beyond 510 °C, there is neither weight loss nor reactions, which indicates the formation of the $\text{La}_{1.5}\text{Pr}_{0.5}\text{Mo}_2\text{O}_9$ phase. Similar thermal behaviour was observed for the other $\text{La}_{2-x}\text{Pr}_x\text{Mo}_2\text{O}_9$ compositions and, therefore, is not reported here.

The structure of the resultant $\text{La}_{2-x}\text{Pr}_x\text{Mo}_2\text{O}_9$ products was investigated by room temperature X-ray diffraction patterns, as

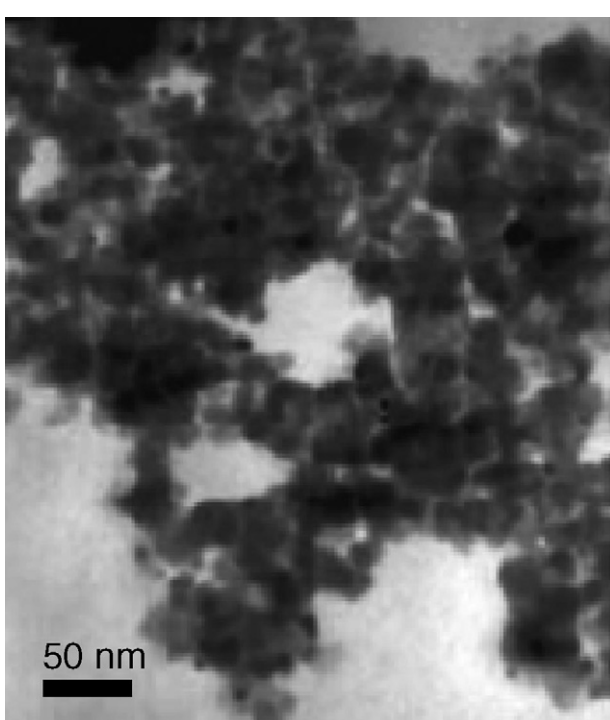


Fig. 4. Transmission electron micrograph of $\text{La}_{1.5}\text{Pr}_{0.5}\text{Mo}_2\text{O}_9$ nanopowder.

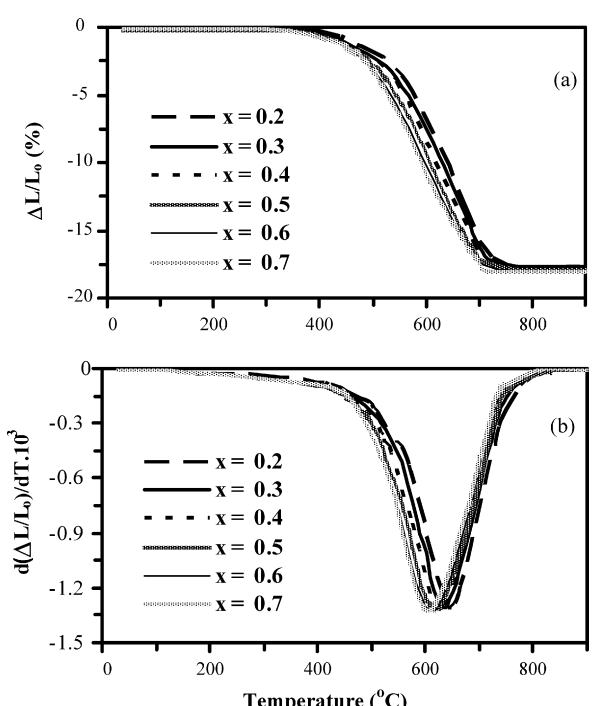


Fig. 6. (a) Shrinkage and (b) shrinkage rate behaviour of $\text{La}_{2-x}\text{Pr}_x\text{Mo}_2\text{O}_9$ samples.

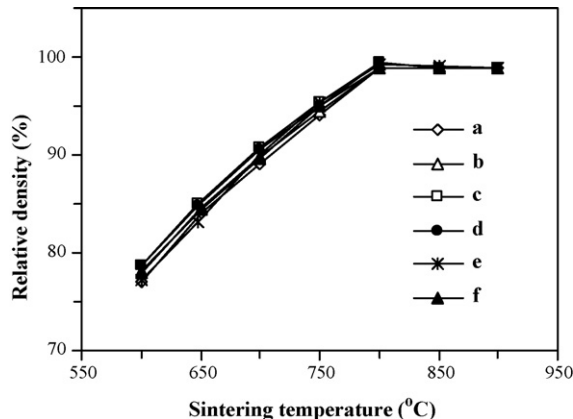


Fig. 7. Relative density of $\text{La}_{2-x}\text{Pr}_x\text{Mo}_2\text{O}_9$ samples isothermally sintered at 600–900 °C for 4 h. (a) $\text{La}_{1.8}\text{Pr}_{0.2}\text{Mo}_2\text{O}_9$; (b) $\text{La}_{1.7}\text{Pr}_{0.3}\text{Mo}_2\text{O}_9$; (c) $\text{La}_{1.6}\text{Pr}_{0.4}\text{Mo}_2\text{O}_9$; (d) $\text{La}_{1.5}\text{Pr}_{0.5}\text{Mo}_2\text{O}_9$; (e) $\text{La}_{1.4}\text{Pr}_{0.6}\text{Mo}_2\text{O}_9$; (f) $\text{La}_{1.3}\text{Pr}_{0.7}\text{Mo}_2\text{O}_9$.

presented in Fig. 2(a–g). The results show well-defined peaks, even at a temperature as low as 510 °C. This finding suggests that the product obtained immediately after decomposition has gained a single-phase structure without any residual impurities (Fig. 2(a–f)). For compositions $x > 0.7$, however, unidentifiable impurity peaks are observed. Thus, the solubility of Pr

in $\text{La}_2\text{Mo}_2\text{O}_9$ is limited to $x = 0.7$. Though $\alpha\text{-La}_2\text{Mo}_2\text{O}_9$ is assumed to have a monoclinic symmetry, distortion is reported and is too small to be observed under normal X-ray investigation [18,24,26,32]. Moreover, most of the reflections of the $\alpha\text{-La}_2\text{Mo}_2\text{O}_9$ phase are comparable to the reflections of the high-temperature cubic β -phase. Hence, the low-temperature α -phase is considered to have a pseudo-cubic symmetry and has been indexed with respect to a cubic symmetry by many investigators [18,24,26,32]. The XRD patterns of the Pr-doped ($x \leq 0.7$) samples appear to be similar to that of the $\beta\text{-La}_2\text{Mo}_2\text{O}_9$ phase. Therefore, the lattice parameters for all compositions were refined on the basis of the cubic symmetry. The variation of the lattice parameters of $\text{La}_{2-x}\text{Pr}_x\text{Mo}_2\text{O}_9$ as a function of Pr content is presented in Fig. 3. As the amount of Pr is increased there is a decrease in the lattice parameter, because of the incorporation of a smaller Pr^{3+} ion ($r = 1.179 \text{ \AA}$) into a larger La^{3+} ($r = 1.216 \text{ \AA}$) lattice site in the $\text{La}_2\text{Mo}_2\text{O}_9$.

A typical TEM image of the synthesized $\text{La}_{1.5}\text{Pr}_{0.5}\text{Mo}_2\text{O}_9$ is presented in Fig. 4. The average particle size of the nanopowder is about $\sim 25 \text{ nm}$.

Phase transitions of the Pr-doped $\text{La}_2\text{Mo}_2\text{O}_9$ samples were studied by means of differential scanning calorimetry; the results are presented in Fig. 5(a–f). Since all the DSC runs are performed with equal masses of samples, the partial substitution of La by Pr does not appear to suppress completely the phase transition. The

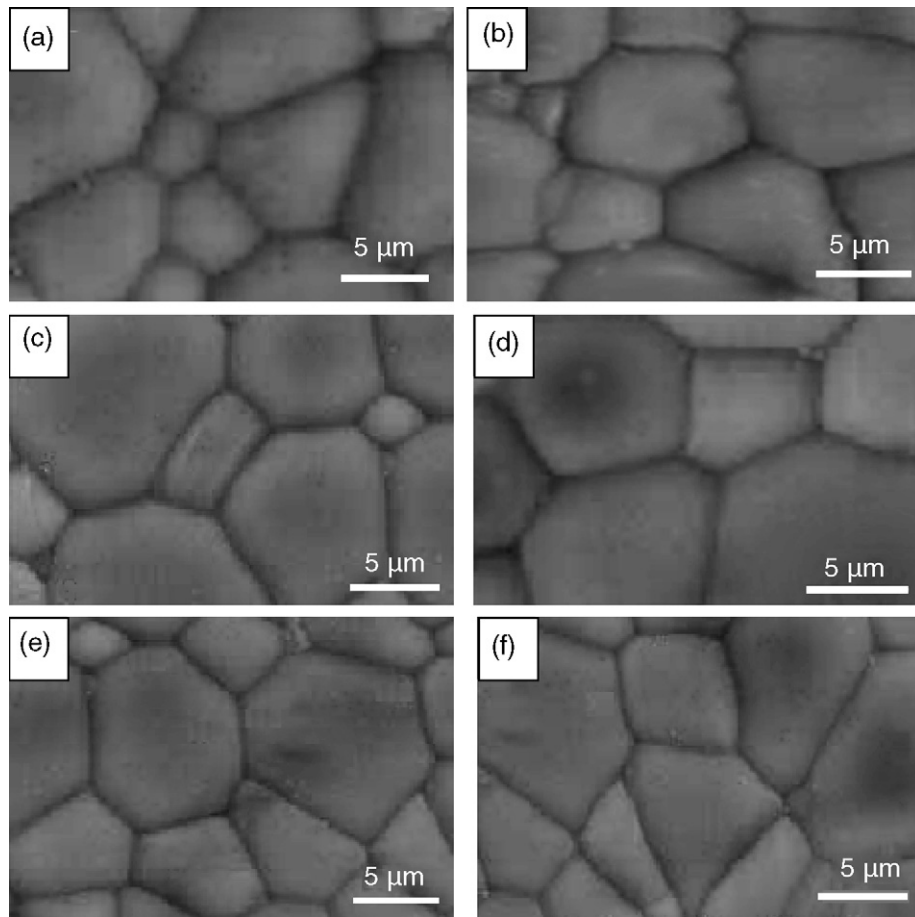


Fig. 8. Scanning electron micrographs of Pr-doped $\text{La}_2\text{Mo}_2\text{O}_9$ pellets sintered at 800 °C for 4 h. (a) $\text{La}_{1.8}\text{Pr}_{0.2}\text{Mo}_2\text{O}_9$; (b) $\text{La}_{1.7}\text{Pr}_{0.3}\text{Mo}_2\text{O}_9$; (c) $\text{La}_{1.6}\text{Pr}_{0.4}\text{Mo}_2\text{O}_9$; (d) $\text{La}_{1.5}\text{Pr}_{0.5}\text{Mo}_2\text{O}_9$; (e) $\text{La}_{1.4}\text{Pr}_{0.6}\text{Mo}_2\text{O}_9$; (f) $\text{La}_{1.3}\text{Pr}_{0.7}\text{Mo}_2\text{O}_9$.

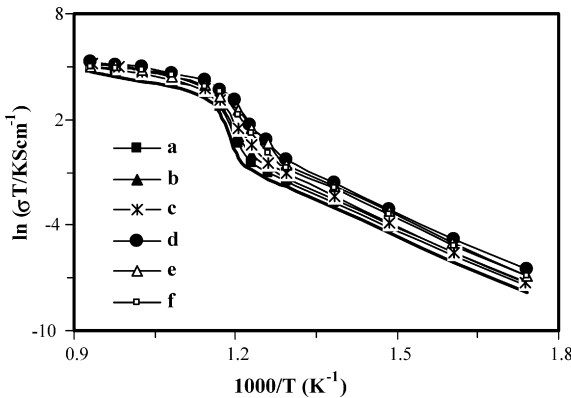


Fig. 9. Arrhenius plots of overall conductivity for $\text{La}_{2-x}\text{Pr}_x\text{Mo}_2\text{O}_9$ samples sintered at 800°C : (a) $\text{La}_{1.8}\text{Pr}_{0.2}\text{Mo}_2\text{O}_9$; (b) $\text{La}_{1.7}\text{Pr}_{0.3}\text{Mo}_2\text{O}_9$; (c) $\text{La}_{1.6}\text{Pr}_{0.4}\text{Mo}_2\text{O}_9$; (d) $\text{La}_{1.5}\text{Pr}_{0.5}\text{Mo}_2\text{O}_9$; (e) $\text{La}_{1.4}\text{Pr}_{0.6}\text{Mo}_2\text{O}_9$; (f) $\text{La}_{1.3}\text{Pr}_{0.7}\text{Mo}_2\text{O}_9$. Dark line shows conductivity of pure $\text{La}_2\text{Mo}_2\text{O}_9$ [31].

phase transition peak becomes small and wide with increasing Pr concentration as evident from Fig. 5(a–f). It is notable that even at higher concentration of Pr ($x=0.7$) is unable to suppress the phase transition completely. However, the phase transition peak is very broad and almost negligible for the $\text{La}_{1.3}\text{Pr}_{0.7}\text{Mo}_2\text{O}_9$ compound.

The sintering properties of the powder compacts were investigated with a dilatometer. The shrinkage and shrinkage rate curves for $\text{La}_{2-x}\text{Pr}_x\text{Mo}_2\text{O}_9$ pellets during heating are shown in Fig. 6. All Pr-doped pellets have similar green densities (61.5–62.8%). In all samples, shrinkage starts at around $\sim 450^\circ\text{C}$, but the maximum densification occurs at $615\text{--}635^\circ\text{C}$. The maximum densification peaks shift slightly towards lower temperatures on increasing the Pr dopant concentration. The sintering process finishes at 800°C for all samples, at which a total shrinkage of 18.1% is recorded and the density is calculated to be greater than 98% of the theoretical value.

The relative density of Pr-doped $\text{La}_2\text{Mo}_2\text{O}_9$ pellets isothermally sintered at $600\text{--}900^\circ\text{C}$ for 4 h is given in Fig. 7. The sinterability of these oxides is obviously good; they can densified to $\sim 99\%$ of theoretical density even at a quite low temperature of 800°C , which agrees well with the dilatometry measurements. The powder doped with Pr exhibits a slightly higher sintered density at the same temperature.

Scanning electron micrographs of all the Pr-doped samples sintered at 800°C are shown in Fig. 8. All the samples are relatively dense and do not show much difference in density. However, Pr doping significantly improves the grain growth. The average grain size of the doped samples is between ~ 4 and $12\ \mu\text{m}$.

Arrhenius plots of the overall conductivity of the $\text{La}_{2-x}\text{Pr}_x\text{Mo}_2\text{O}_9$ samples sintered at 800°C is shown in Fig. 9 and conductivity data for pure $\text{La}_2\text{Mo}_2\text{O}_9$ is also given for the purpose of comparison [31]. For pure $\text{La}_2\text{Mo}_2\text{O}_9$, a dramatic change of conductivity occurs at around 560°C and is due to a phase transition. The Pr-doped $\text{La}_2\text{Mo}_2\text{O}_9$ samples exhibit slightly improved conductivity at lower and higher temperatures. Generally, the higher the unit-cell free volume in the oxide-ion conductor is easier for the oxygen-ion diffu-

sion [33,9]. The ionic radius of Pr^{3+} ($r=1.179\text{ \AA}$) is smaller than that of La^{3+} ($r=1.216\text{ \AA}$). On Pr-doping, the cell parameter is decreased. Thus, the substitution of Pr greatly increases the free volume and, therefore, the ionic conductivity of Pr-doped samples also increases remarkably. It can also be seen that a sharp conduction increase is present up to $x=0.5$ in $\text{La}_{2-x}\text{Pr}_x\text{Mo}_2\text{O}_9$. The $\text{La}_{1.5}\text{Pr}_{0.5}\text{Mo}_2\text{O}_9$ sample exhibits a conductivity of 0.165 S cm^{-1} at 800°C , compared with 0.12 S cm^{-1} for the undoped $\text{La}_2\text{Mo}_2\text{O}_9$ [31]. This result confirms that Pr doping can improve the oxide-ion conductivity of $\text{La}_2\text{Mo}_2\text{O}_9$, both at low and high temperatures. Moreover, the high purity and phase homogeneity of the present sample could help to improve the conductivity of Pr-doped $\text{La}_2\text{Mo}_2\text{O}_9$ samples.

4. Conclusions

Nanocrystalline $\text{La}_{2-x}\text{Pr}_x\text{Mo}_2\text{O}_9$ ($0.2 \leq x \leq 0.8$) powders have been successfully synthesized by the pyrolysis of polyacrylate La–Pr–Mo precursors obtained via *in situ* polymerization of metal salts and acrylic acid. Thermal analysis indicates that the Pr-doped $\text{La}_2\text{Mo}_2\text{O}_9$ undergoes complete crystallization at 510°C . X-ray diffraction analysis reveals that the substitution of La by Pr preserves the $\text{La}_2\text{Mo}_2\text{O}_9$ structure up to $x \leq 0.7$. Differential scanning calorimetry shows that Pr doping does not suppress the $\alpha \rightarrow \beta$ phase transition completely, but significantly lowers the transition temperature. Moreover, the synthesized nanocrystalline Pr-doped $\text{La}_2\text{Mo}_2\text{O}_9$ samples have good sinterability. A relatively low sintering temperature of 800°C for 4 h is sufficient to achieve $\sim 99\%$ of theoretical density with a good microstructure. The oxide-ion conductivity increases with increasing Pr content and maximum conductivity is attained at $x=0.5$ in $\text{La}_{2-x}\text{Pr}_x\text{Mo}_2\text{O}_9$.

Acknowledgement

The authors thank Prof. T. Vasudevan, Head, Dept. of Industrial Chemistry, for his constant encouragement and support.

References

- [1] J.P.P. Huijsmans, Curr. Opin. Solid State Mater. Sci. 5 (2001) 317.
- [2] S.P.S. Badwal, F.T. Ciacchi, Adv. Mater. 13 (2001) 993.
- [3] P.N. Dyer, R.E. Richards, S.L. Russek, D.M. Taylor, Solid State Ionics 134 (2000) 21.
- [4] H.L. Tuller, H. Tuller, J. Schoonman, I. Riess (Eds.), Oxygen Ion and Mixed Conductors and Their Technological Applications, Kluwer Academic Publishing, Dordrecht, 2000, p. 245 (NATO ASI series).
- [5] B. Zhu, X.T. Yang, J. Xu, Z.G. Zhu, S.J. Ji, M.T. Sun, J.C. Sun, J. Power Sources 118 (2003) 47.
- [6] H.T. Liu, R.F. Chen, X.Q. Song, Chin. J. Chem. 20 (2002) 1536.
- [7] J.B. Goodenough, A. Manthiram, P. Paramthaman, Y.S. Zhen, Solid State Ionics 52 (1992) 105.
- [8] M. Feng, J.B. Goodenough, Eur. J. Solid State Inorg. Chem. 31 (1994) 663.
- [9] T. Ishihara, H. Matsuda, Y. Takita, J. Am. Chem. Soc. 116 (1994) 3801.
- [10] H. Arai, Bull. Ceram. Soc. Jpn. 27 (1992) 100.
- [11] K.Q. Huang, M. Feng, J.B. Goodenough, J. Am. Ceram. Soc. 81 (1998) 357.
- [12] D.P. Fagg, J.C.C. Abrantes, D. Perez-Coll, P. Nunez, V.V. Kharton, J.R. Frade, Electrchim. Acta 48 (2003) 1023.

- [13] F. Abraham, M.F. Debureille-Gresse, G. Mairesse, G. Nowogrocki, Solid State Ionics 28 (1988) 523.
- [14] F. Abraham, J.C. Boivin, G. Mairesse, G. Nowogrocki, Solid State Ionics 28–30 (1990) 529.
- [15] S.A. Kramer, H.L. Tuller, Solid State Ionics 82 (1995) 15.
- [16] H.L. Tuller, Solid State Ionics 94 (1997) 63.
- [17] P. Lacorre, F. Goutenoire, O. Bohnke, R. Retoux, Y. Laligant, Nature 404 (2000) 856.
- [18] F. Goutenoire, O. Isnard, R. Retoux, P. Lacorre, Chem. Mater. 12 (2000) 2575.
- [19] P. Lacorre, Solid State Sci. 2 (2000) 755.
- [20] F. Goutenoire, O. Isnard, E. Suard, O. Bohnke, Y. Laligant, R. Retoux, P. Lacorre, J. Mater. Chem. 11 (2001) 119.
- [21] X.P. Wang, Q.F. Fang, Z.S. Li, G.G. Zhang, Z.G. Yi, Appl. Phys. Lett. 81 (2002) 3434.
- [22] J.A. Collado, M.A.G. Aranda, A. Cabeza, P. Olivera-Pastor, S. Bruque, J. Solid State Chem. 167 (2002) 80.
- [23] S. Georges, G. Goutenoire, F. Altörfer, D. Sheptyakov, F. Fauth, E. Suard, P. Lacorre, Solid State Ionics 161 (2003) 231.
- [24] S. Georges, F. Goutenoire, Y. Laligant, P. Lacorre, J. Mater. Chem. 13 (2003) 2317.
- [25] R. Subasri, D. Matusch, H. Nafe, F. Aldinger, J. Eur. Ceram. Soc. 24 (2004) 129.
- [26] S.A. Hayward, S.A.T. Redfern, J. Phys. Condens. Matter 16 (2004) 3571.
- [27] Z.S. Khadasheva, N.U. Venskovskii, M.G. Safronenko, A.V. Mosunov, E.D. Politova, S.Yu. Stefanovich, Inorg. Mater. 38 (2002) 1168.
- [28] I.P. Marozau, D. Marrero-Lopez, A.L. Shaula, V.V. Kharton, E.V. Tsipis, P. Nunez, J.R. Frade, Electrochim. Acta 49 (2004) 3517.
- [29] C. Tealdi, G. Chiadelli, L. Malavasi, G. Flor, J. Mater. Chem. 14 (2004) 3553.
- [30] D. Marrero-Lopez, J. Canales-Vazquez, J.C. Ruiz-Morales, J.T.S. Irvine, P. Nunez, Electrochim. Acta 50 (2005) 4385.
- [31] A. Subramania, T. Saradha, S. Muzhumathi, T. Vasudevan, Proceedings of the Seventh European SOFC Forum, 2006, P0519.
- [32] A. Arulraj, F. Goutenoire, M. Tabellout, O. Bohnke, Y. Laligant, R. Retoux, P. Lacorre, Chem. Mater. 14 (2002) 2492.
- [33] H. Yammura, K. Matsui, K. Kakinuma, T. Mori, Solid State Ionics 123 (1999) 279.